1 **CSF1R inhibition by PLX5622 reduces pulmonary fungal infection**

2 **by depleting MHCIIhi interstitial lung macrophages**

3 Sally H. Mohamed[1], Eliane Vanhoffelen[2], Man Shun Fu[1], Emilie Cosway[1], Graham

4 Anderson[1], Greetje Vande Velde[2], Rebecca A. Drummond[1, 3]*

5

6 [1]Institute of Immunology & Immunotherapy, University of Birmingham, UK

7 [2]Department of Imaging and Pathology, Biomedical MRI/MoSAIC, KU Leuven, Leuven,

8 Belgium

9 [3]Institute of Microbiology & Infection, University of Birmingham, UK

10

11 *correspondence: r.drummond@bham.ac.uk

12

13

14 **Abstract**

15 PLX5622 is a small molecular inhibitor of the CSF1 receptor (CSF1R) and is widely used to

16 deplete macrophages within the central nervous system (CNS). However, recent reports

17 have indicated that PLX5622 may affect myeloid cells in other organs including the bone

18 marrow and spleen. We investigated the impact of PLX5622 treatment in wild-type C57BL/6

19 mice and discovered that one-week treatment with PLX5622 was sufficient to deplete

20 interstitial macrophages in the lung and brain-infiltrating Ly6C^{low} patrolling monocytes, in

21 addition to CNS-resident macrophages. These cell types were previously indicated to act as

22 infection reservoirs for the pathogenic fungus *Cryptococcus neoformans*. We therefore took

23 advantage of PLX5622-mediated depletion of these myeloid cell subsets to examine their

24 functional role in *C. neoformans* lung infection and extrapulmonary dissemination. We found

25 that PLX5622-treated mice had significantly reduced fungal lung infection and reduced

26 extrapulmonary dissemination to the CNS but not to the spleen or liver. Fungal lung infection

27 mapped to MHCII^{hi} interstitial lung macrophages, which underwent significant expansion

1

28   during infection following monocyte replenishment and not local division. Although PLX5622

29   depleted CNS infiltrating patrolling monocytes, these cells did not accumulate in the fungal-

30   infected CNS following pulmonary infection. In addition, Nr4a1-deficient mice, which lack

31   patrolling monocytes, had similar control and dissemination of *C. neoformans* infection to

32   wild-type controls. Our data demonstrate that PLX5622 may have a beneficial effect in the

33   control of intracellular replicating pathogenic fungi that utilise CSF1R-dependent myeloid

34   cells as infection reservoirs.

Introduction

Myeloid cell population size is predominantly controlled by the growth factor CSF1 (M-CSF) [1]. Expression of the CSF1 receptor (CSF1R) broadly identifies the myeloid lineage, but is particularly highly expressed by neutrophils, monocytes and macrophages [2]. Different subsets of macrophages and monocytes exhibit varying degrees of sensitivity to CSF1, which appears to correlate with the dependency on CSF1R for survival [2]. For example, maintenance and development of central nervous system (CNS)-resident microglia is highly dependent on the CSF1R, since mutation or deletion of this receptor results in complete ablation of microglia numbers in rodents and humans [3-5]. In the lung, alveolar and interstitial macrophages express similar levels of CSF1R but have divergent uptake rates of CSF1, with interstitial macrophages more readily responsive to CSF1 stimulation [2]. However, genetic deletion of CSF1R in mice and rats does not reduce total numbers of lung macrophages [3, 5].

Since CNS-resident macrophages are highly dependent on CSF1R signalling for survival, chemical inhibitors of CSF1R are an effective tool to deplete these macrophage populations [6]. The most specific CSF1R inhibitor is PLX5622, which has greater brain penetrance than other CSF1R inhibitors (e.g. PLX3397) [7, 8]. When given orally, PLX5622 rapidly depletes CNS-resident macrophages (including parenchymal microglia and border macrophage populations) [8]. Several studies have used PLX5622-treatment models to demonstrate the critical role of microglia in controlling CNS infections and neuroinflammation [8-10]. However, controversy over the specificity of PLX5622 has emerged in recent years [11, 12]. One study showed that PLX5622 caused significant alterations to both myeloid and lymphoid populations within the spleen and bone marrow, and macrophages derived from the bone marrow of PLX5622-treated mice had impaired production of IL-1β [11]. Many of these effects remained 3 weeks after PLX5622 treatment had stopped, indicating at long-term consequences of disrupting CSF1R-dependent myeloid compartments [11]. In other studies, monocyte numbers were reduced by PLX5622 treatment although these effects may

62   be subset and context specific [10, 13, 14], since other studies have found no effect on

63   either monocyte or non-CNS macrophage numbers [15, 16].

64   Tissue-resident macrophages and monocytes are integral to the pathogenesis of the

65   fungal infection caused by *Cryptococcus neoformans* [17]. This opportunistic fungal

66   pathogen causes lung infections and life-threatening meningitis in patients with

67   compromised T-cell immunity. Cryptococcal meningitis causes 19% of all AIDS-related

68   deaths globally [18]. Macrophages and monocytes have a poor capacity to kill *C.*

69   *neoformans* without the help of IFNγ-producing CD4 T-cells. In the absence of Th1 immunity,

70   monocytes and macrophages are susceptible to intracellular infection, marked by strong

71   upregulation of arginase and an 'M2' like functional phenotype [17]. *C. neoformans*-infected

72   monocytes are thought to contribute towards dissemination of the infection, especially to the

73   brain and CNS [19, 20]. Tissue-resident macrophages are also an important reservoir for *C.*

74   *neoformans* in both the brain and lung. We recently found that targeted microglia depletion

75   could reduce fungal brain infection, since microglia shielded *C. neoformans* from copper

76   starvation within the CNS [21]. In the lung, *C. neoformans* produces a secreted peptide

77   called CPL-1 that drives arginase expression within interstitial macrophages to promote

78   intracellular growth [22]. The ability of this fungus to access and infect monocytes and

79   macrophages is therefore critical for the infection lifecycle.

80   In the present work, we characterised the impact of PLX5622 treatment on numbers

81   of myeloid cells in the CNS, spleen, lung, blood and bone marrow. We discovered that while

82   PLX5622 primarily depleted CNS-resident macrophages, there was additional specific

83   depletion of CNS-infiltrating patrolling monocytes and lung interstitial macrophages. Since

84   these myeloid populations were previously implicated in the pathogenesis of *C. neoformans*

85   infection, we investigated whether PLX5622 could have a therapeutic effect for this fungal

86   infection and explored the functional roles of these cells during lung infection and

87   extrapulmonary dissemination.

88   **Results**

89

90   **Interstitial lung macrophages are depleted by PLX5622**

91   PLX5622 is used to deplete tissue-resident macrophages within the CNS that are highly

92   dependent on CSF1R signalling for survival [6]. However, some reports have suggested that

93   PLX5622 treatment has off-target effects, particularly within the spleen, bone marrow and

94   lung [11]. To independently verify those results, we measured the number of macrophages

95   in brains, meninges, spleens, bone marrow and lungs of mice given control diet or high

96   concentration (1200 ppm) PLX5622 diet for 1 week, using flow cytometry (Fig S1). We found

97   that PLX5622-treated mice had more than 90% loss of microglia and other CNS-resident

98   macrophages (Fig 1A), as previously described. In addition, we also found a significant loss

99   of splenic macrophages in the PLX5622-treated animals (Fig 1B), but no effect on

100   macrophages within the bone marrow (Fig 1C). In the lung, we found that PLX5622

101   specifically depleted interstitial macrophages whereas alveolar macrophage numbers were

102   unaffected (Fig 1D). Taken together, our data show that high dose PLX5622 has the most

103   profound effect on CNS-resident macrophages but also depletes splenic and interstitial lung

104   macrophages.

105

106   **PLX5622 depletes patrolling monocytes in an organ-specific manner**

107   Monocytes are a heterogeneous group of circulating myeloid cells. The two major functional

108   classes of these are classical inflammatory monocytes (Ly6C^{hi} in mice) or non-classical

109   patrolling monocytes (Ly6C^{low}) [23]. Some studies have indicated that PLX5622 induces

110   depletion of both or one of these monocyte subsets [10, 13, 14], while others have observed

111   no effect on either subset [15, 16]. To determine whether PLX5622 causes loss of

112   monocytes at the steady-state, we quantified the number of Ly6C^{hi} classical monocytes and

113   Ly6C^{low} patrolling monocytes in the blood, lung, spleen, bone marrow and CNS after 1 week

114   of PLX5622 treatment. We found that PLX5622 had no effect on the number of circulating

115   monocytes in the blood, lung, spleen or bone marrow (Fig 2A-D). In contrast, we found a

116   significant depletion of Ly6C^{low} monocytes in the brain of PLX5622-treated mice (Fig 2E), but

117   no effect in the meninges (Fig 2F). Classical Ly6C^{hi} monocytes remained similar to untreated

118   controls in all tissues examined (Fig 2). Our data show that CNS-infiltrating Ly6C^{low} patrolling

119   monocytes are depleted by PLX5622, which may be secondary to microglia depletion as

120   circulating monocytes were unaffected.

121

122   **PLX5622 reduces fungal lung infection**

123   As we had found that PLX5622 specifically depleted interstitial macrophages in the lung, we

124   took advantage of this to examine the functional role of these cells in *C. neoformans* lung

125   infection, in which interstitial macrophages were recently identified as an infection reservoir

126   [22]. We treated wild-type mice with PLX5622 for 1 week and then performed an intranasal

127   infection with *C. neoformans* prior to measuring fungal burdens in the lung at day 21 post-

128   infection (Fig 3A). We found that PLX5622-treatment led to a significant reduction in lung

129   fungal burden (Fig 3B) and to a non-significant reduction in lung lesion volume (Fig S2), but

130   had no effect on the recruitment of inflammatory cells to the infected lung including

131   monocytes, neutrophils and eosinophils (Fig 3C). We also found no difference in the

132   numbers of lymphocytes, either at steady-state or following infection (Fig 3D). Lymphocyte

133   numbers were also unaffected in the blood, bone marrow and spleen of PLX5622-treated

134   mice (Fig S3). PLX5622-induced depletion of interstitial macrophages was maintained up to

135   day 21 post-infection (Fig 3C) with no effect observed on alveolar macrophages, both in

136   number (Fig 3C) and their expression of activation markers MHCII and F480 (Fig S4).

137   PLX5622 also did not directly have an antifungal effect, as yeast grown in PLX5622 (at

138   concentrations previously measured in brain and serum of treated mice [24]) grew similarly

139   to untreated yeast cultures (Fig S5). Taken together, this data shows that PLX5622

140   treatment reduces fungal lung infection, which is correlated with a specific loss of interstitial

141   macrophages.

142

143   **Extrapulmonary dissemination to the CNS is reduced by PLX5622 treatment**

144   Previous work has shown that the rate of lung infection can determine the kinetics of

145   extrapulmonary dissemination to the CNS [25]. Since we had observed that PLX5622

146   reduced fungal lung infection (Fig 3B), we measured fungal burdens in other tissues to

147   examine the effect of PLX5622 treatment on fungal dissemination from the lung. After day 21

148   post-intranasal infection, we found that fungal burdens in the brain were significantly reduced

149   in PLX5622-treated animals compared to untreated controls (Fig 4A). In contrast,

150   extrapulmonary dissemination to the spleen and liver were unaffected by PLX5622 treatment

151   (Fig 4A). In the brain, PLX5622-treated mice had significantly reduced numbers of microglia

152   and macrophages (Fig 4B) similar to uninfected mice (Fig 1A). Numbers of recruited

153   inflammatory cells (neutrophils, inflammatory monocytes) were unaffected by PLX5622

154   treatment (Fig 4B). Numbers of patrolling Ly6C^{low} monocytes were reduced in the infected

155   brains of PLX5622-treated mice (Fig 4B), similar to what we observed in uninfected mice.

156   We recently showed that microglia support *C. neoformans* brain infection by acting

157   as a fungal reservoir during acute meningitis (intravenous infection) [21]. Loss of microglia in

158   the PLX5622-treated mice may therefore cause a reduction in brain fungal burdens by

159   removing this growth niche, in addition to reduced extrapulmonary dissemination from the

160   lung, or the loss of microglia independently reduces brain fungal burden (as we previously

161   observed in the intravenous infection model). To explore these possibilities, we first

162   correlated lung and brain fungal burdens in the same mice to determine whether higher lung

163   burdens predicted greater brain infection (and thus increased extrapulmonary

164   dissemination). Indeed, we found that mice with higher lung infection had greater brain

165   infection, and PLX5622 treatment did not disrupt this relationship (Fig 4C). These data

166   indicate that PLX5622-treated mice had reduced brain infection due to reduced lung

167   burdens, although we cannot rule out an additional independent effect of microglia depletion

168   on control of brain infection. Taken together, these data show PLX5622 treatment causes a

169   reduction in extrapulmonary dissemination to the CNS but not to the spleen or liver.

170

171   ***C. neoformans* preferentially infects MHCII^{hi} lung interstitial macrophages**

172   Since PLX5622 specifically depleted interstitial macrophages in the lung and this correlated

173   with a reduction in lung infection and dissemination to the CNS, we further characterised

174   these cells in response to *C. neoformans* infection. Lung interstitial macrophages comprise a

175   heterogeneous population of different functional subsets, some which associate with nerve

176   bundles and others with blood vessels [26, 27]. We used MHC Class II to subdivide

177   interstitial macrophages into two subsets (Fig 5A) and analysed their responses to fungal

178   infection. There was a greater number and ratio of MHCII^{hi} interstitial macrophages in the

179   lung, both at the steady-state and during fungal infection (Fig 5B). We found that both

180   subsets of interstitial macrophages expanded at day 21 post-*C. neoformans* infection,

181   although this only achieved statistical significance for the MHCII^{hi} subset (Fig 5B). PLX5622

182   treatment significantly ablated the MHCII^{hi} interstitial macrophages, and had less of an

183   impact on the less numerous MHCII^{low} interstitial macrophages (Fig 5C).

184   We next examined the interaction of interstitial macrophages with fungi following

185   infection, using mCherry-expressing *C. neoformans* to track its localisation to different

186   myeloid cell populations in the lung after intranasal infection (Fig 5D). These experiments

187   revealed that *C. neoformans* primarily localised within interstitial macrophages compared to

188   alveolar macrophages when the frequency of detected yeast cells was higher (>0.05% total

189   lung events) (Fig 5E). In contrast, mice with a lower fungal lung burden (<0.05% of total lung

190   events) had a greater proportion of uptake by alveolar macrophages compared to interstitial

191   macrophages (Fig 5E). These data indicate that interstitial macrophages may be more

192   susceptible to intracellular infection, which promotes a greater level of infection. To test that,

193   we measured expression of arginase using intracellular flow cytometry, since arginase-

194   expressing macrophages have been previously shown to support intracellular fungal growth

195   and have poor killing capacity. Indeed, we found that arginase expression was dramatically

196   increased in interstitial macrophages following infection compared to alveolar macrophages

197   (Fig 5F), supporting recent work that also found interstitial macrophages were primarily

198   susceptible to intracellular fungal infection via arginase induction [22]. Next, we examined

199   which interstitial macrophage subset had greater uptake/association with *C. neoformans*. We

8

200 found that MHCII^{hi} interstitial macrophages were the predominant subset interacting with

201 fungi, regardless of the total frequency of infected cells (Fig 5G). In line with that, MHCII^{hi}

202 interstitial macrophages expressed higher levels of arginase than MHCII^{low} interstitial

203 macrophages (Fig 5G). Taken together, our data show that MHCII^{hi} interstitial macrophages

204 undergo a significant expansion following *C. neoformans* infection and that these cells are

205 susceptible to intracellular infection.

206

207 **Interstitial macrophage expansion is driven by monocytes and not local proliferation**

208 As we had observed increases in the size of the interstitial macrophage population in

209 response to fungal infection, we sought to understand the main driver of this expansion.

210 Type-2 cytokines such as IL-4 can promote macrophage proliferation [28] and type-2

211 immune responses are a key feature of *C. neoformans* lung infections. Indeed, we also

212 observed increases in the concentration of IL-4 and IL-13 in the lung following infection (Fig

213 S6). However, *C. neoformans* intracellular infection can also introduce cell cycle blocks in

214 macrophages [29]. We therefore measured interstitial macrophage proliferation in the

215 uninfected and infected lung using Ki67 as a marker for dividing cells. In uninfected mice, we

216 found little proliferation occurring in alveolar macrophages and eosinophils, with a greater

217 proportion of interstitial macrophages staining positive for Ki67 at baseline (Fig 6A). Upon

218 infection, we found that this level significantly decreased, for both eosinophils and interstitial

219 macrophages (Fig 6A). The level of proliferation did not significantly differ between MHCII^{low}

220 and MHCII^{hi} interstitial macrophage subsets (Fig S7). Therefore, the expansion of interstitial

221 macrophages is not driven by proliferation, and instead fungal infection decreases the

222 baseline proliferation of these cells. In line with that, we found no difference in the type-2

223 response between untreated and PLX5622-treated lungs, measured either by total IL-4/13 in

224 lung homogenates (Fig S6) or by eosinophil recruitment (Fig 3C).

225 Since proliferation was not the main driver of interstitial macrophage expansion during

226 fungal infection, we instead examined whether monocytes differentiating into interstitial

227 macrophages were the primary cause of interstitial macrophage expansion. For that, we

228   used *Cx3cr1-GFP-Ccr2-RFP* mice to track expression of tissue-resident (CX3CR1) and

229   monocyte (CCR2) markers in interstitial macrophages during fungal lung infection. At

230   baseline, MHCII^{hi} interstitial macrophages were mostly CX3CR1^{+}CCR2^{-} (tissue-resident)

231   with a smaller population of CX3CR1^{+}CCR2^{+} monocyte-derived cells (Fig 6B). In contrast,

232   MHCII^{low} interstitial macrophages lacked a CCR2^{+} population, indicating that monocytes are

233   not a significant contributor to this population (Fig 6B). We did not detect CX3CR1 or CCR2

234   expression in alveolar macrophages or eosinophils (Fig S8). After fungal infection, we found

235   a population of CX3CR1^{low}CCR2^{+} cells emerged in both interstitial macrophage subsets (Fig

236   6B), which likely represents immature monocyte-derived cells that contribute to the interstitial

237   macrophage pool in the lung following infection.

238   Taken together, our data show that the interstitial macrophage population dynamically

239   changes in response to fungal infection, undergoing monocyte-driven expansions that may

240   be driven by reduced capacity to proliferate as a result of intracellular infection.

241

242   **Patrolling monocytes play a minor role in extrapulmonary dissemination of *C.***

243   ***neoformans***

244   Patrolling monocytes were recently shown to act as Trojan Horses and drive dissemination

245   of *C. neoformans* into the CNS [19]. These studies were completed using an intravenous

246   model of infection [23], and therefore the role of patrolling monocytes in extrapulmonary

247   dissemination is unclear. Our data showed that PLX5622 caused a depletion of patrolling

248   monocytes within the CNS (Fig 2), raising the possibility that the reduction in fungal burdens

249   we observed in this tissue may in part be caused by a reduction in Trojan Horse-driven

250   dissemination within patrolling monocytes. To explore this possibility, we first measured

251   recruitment of patrolling monocytes to the CNS after intranasal infection. We found no

252   significant increase in the number of patrolling monocytes in the brain or meninges at

253   several time points post-intranasal infection (Fig 7A). Next, we used mice lacking patrolling

254   monocytes to determine the role of these cells for anti-cryptococcal immunity following

255   pulmonary infection. Nr4a1 (Nur77) is a transcription factor that controls the development of

10

256   patrolling monocytes [30]. Mice lacking Nr4a1 have significantly reduced circulating

257   patrolling monocytes [30], which we confirmed in our mice (Fig 7B). *Nr4a1*$^{-/-}$ mice can

258   therefore be used to assess the contribution of patrolling monocytes for the control of *C.*

259   *neoformans* infection. We intranasally infected these animals with *C. neoformans* and

260   measured fungal burdens in the brain and lungs at 21 days post-infection. We found no

261   significant differences between *Nr4a1*$^{-/-}$ mice and wild-type controls in control of lung or brain

262   infection in either of these organs (Fig 7C). Taken together, we conclude that patrolling

263   monocytes therefore play a redundant role in dissemination and control of *C. neoformans*

264   infection following intranasal administration.

Discussion

Intracellular survival within monocytes and macrophages is a critical part of the *C. neoformans* infection lifecycle. Understanding the factors that influence fungal intracellular residence has been a core goal for developing new treatment strategies for this infection, which are urgently needed because cryptococcal meningitis now accounts for 19% of all AIDS-related deaths globally [18]. In the current work, we found that depletion of CNS and lung resident macrophages with high dose PLX5622 treatment reduced *C. neoformans* infection. PLX5622 limited fungal infection within MHCII^{hi} interstitial lung macrophages, which expanded during infection following monocyte replenishment.

PLX5622 is primarily used to deplete CNS-resident macrophages, since microglia (and other types of CNS-resident macrophages) are highly dependent on the CSF1R for survival [31]. Rodents deficient in CSF1R lack these brain macrophages [3, 5], and a recent case report illustrated that human mutations in *CSF1R* resulted in complete loss of microglia and a consequent lethal disruption to brain development [4]. We recently demonstrated that targeted microglia depletion reduced *C. neoformans* infection in the CNS in a model of acute meningitis that bypassed pulmonary immunity [21]. In the current work, we used an intranasal infection model where yeast infection disseminates from the lung to other organs following breakdown of pulmonary barrier immunity. We found that loss of microglia in the CNS equated to reduced fungal brain infection, validating our earlier observations in the acute infection model [21]. However, further examination of PLX5622-treated mice revealed that fungal infection was also reduced in the lung, which may have exaggerated the reduced fungal brain burden by reducing the rate of extrapulmonary dissemination. Indeed, we found strong correlation between lung and brain burden in this model, in line with other reports [25]. Therefore, while microglia may support *C. neoformans* infection in the brain following intranasal infection, the therapeutic effect we observed with PLX5622 treatment may be enhanced by additional effects on dissemination patterns caused by PLX5622-mediated depletion of non-CNS myeloid cells.

292   Extrapulmonary dissemination of *C. neoformans* is further influenced by fungal

293   morphotype. In the lung, *C. neoformans* forms large cells termed titan cells that are unable

294   to be phagocytosed [32, 33]. As infection progresses, *C. neoformans* forms small cells that

295   have greater propensity to disseminate to the brain, spleen and liver [34]. These small cells,

296   called seed cells, were recently shown to have greater survival and accumulation within the

297   CNS following pulmonary infection [34]. Whether PLX5622 affects *C. neoformans*

298   morphotype in the lung and brain was not explored, although we did not observe any impact

299   of PLX5622 on *C. neoformans* growth at a range of physiological concentrations that were

300   previously measured in mice treated with high dose PLX5622 [24].

301   Dissemination of *C. neoformans* from the lung to other body sites is partially

302   mediated by circulating monocytes [20]. Early experiments showed that infection of mice

303   with *C. neoformans*-infected monocytes resulted in greater dissemination rates compared to

304   mice infected with yeast alone [35], indicating that fungal-infected monocytes are better

305   equipped to enter tissues and spread infection. Indeed, $Ly6C^{low}$ patrolling monocytes were

306   shown to carry *C. neoformans* into the CNS vasculature and contribute towards brain

307   infection via a mechanism that required TNFR signalling [19]. That study used an

308   intravenous model of infection, but the role of patrolling monocytes in promoting brain

309   infection using other infection routes was not explored. We found that PLX5622 depleted

310   patrolling monocytes specifically within the brain but not in the blood or other tissues. Other

311   studies have also reported a depletion of monocytes within the CNS [10, 14]. Monocytes

312   circulating in the blood do not appear to be affected by PLX5622 treatment, either in our

313   study or in others [10, 16]. Taken together, these findings suggest that PLX5622 may not

314   deplete $Ly6C^{low}$ monocytes directly, but that the recruitment of these cells into the CNS may

315   depend on the presence of microglia and CNS border macrophages. Since PLX5622-treated

316   mice had reduced patrolling monocytes in the CNS, we tested whether this contributed

317   towards the reduction in brain fungal burdens. However, we found that patrolling monocytes

318   are not a significant driver of dissemination to the CNS following intranasal *C. neoformans*

319   infection. Mice lacking Nr4a1 (which controls patrolling monocyte development [30]) were

13

320   not better protected from infection, nor did we see any measurable accumulation of this

321   monocyte subset in the CNS following intranasal infection. Therefore, the involvement of

322   monocyte subsets in *C. neoformans* dissemination and infection may depend on route of

323   infection and is an important consideration for future studies examining *C. neoformans*

324   infection kinetics and the role myeloid cells play in shaping these patterns.

325   Inflammatory Ly6C^{hi} monocytes can also promote *C. neoformans* infections,

326   particularly within the lung. Targeted depletion of CCR2-dependent inflammatory monocytes

327   reduced fungal lung infection (following intratracheal instillation) and prevented

328   dissemination to draining lymph nodes and had a moderate effect on brain dissemination

329   [36]. The specific mechanism by which inflammatory monocytes enhance *C. neoformans*

330   lung infection is unclear, but did not depend on adaptive immunity, eosinophils or arginase

331   induction [36]. It is possible that by targeting monocytes, the replenishment and expansion of

332   lung-resident macrophages was altered in these studies, which may have influenced lung

333   fungal burdens. Indeed, total macrophages and dendritic cells were depleted in the lungs of

334   CCR2-deficient mice [36]. We found that interstitial macrophages, particularly the MHCII^{hi}

335   subset, significantly expanded during infection which was driven by monocytes since local

336   proliferation of interstitial macrophages was decreased during infection. Our understanding

337   of the ontogeny of interstitial macrophages is still evolving, but appears to require low levels

338   of monocyte replenishment that increases with age and/or inflammation [37]. Indeed, the

339   lung macrophage pool dynamically changes following infection as a result of monocyte

340   infiltration, resulting in significant remodelling of the macrophage population that can

341   influence responses to subsequent injuries [38].

342   We found that MHCII^{hi} interstitial macrophages were particularly susceptible to

343   intracellular infection with *C. neoformans*, which correlated with a significant upregulation of

344   arginase in this subset. This data independently validates recent findings from Madhani and

345   colleagues who demonstrated that a *C. neoformans* secreted peptide termed CPL-1 was a

346   strong inducer of arginase and M2 functional polarisation, particularly of lung interstitial

347   macrophages [22]. We found that intracellular infection and arginase induction mapped to

14

348 the MHCII[hi] subset of interstitial macrophages. Functional interstitial macrophage subsets

349 have now been described in multiple studies, which largely agree on the existence of

350 MHCII[hi] and MHCII[low] interstitial macrophages [26, 27, 39]. MHCII[low] interstitial macrophages

351 co-express Lyve1 and CD206, primarily localise around blood vessels and appear to be

352 critical regulators of inflammation and fibrosis since their absence exacerbates lung injury

353 and leukocyte recruitment [39]. MHCII[hi] interstitial macrophages appear to reside near

354 nerves in the lung [26], although there is some variation in reported findings about the

355 localisation and function of these cells [27] which may be due to a lack of consensus on the

356 best way to identify and define interstitial macrophage subsets [37].

357   In our study, we found that treatment with high dose PLX5622 caused specific

358 depletion of interstitial macrophages in the lung, particularly the MHCII[hi] subset. Other

359 studies have also reported potential effects of PLX5622 on lung macrophage populations

360 although characterisation of specific subpopulations were not examined in those studies

361 [11]. In contrast to our findings with PLX5622, mice deficient in CSF1R do not have

362 significant alterations in lung macrophage populations [3, 5]. It is therefore likely that the

363 PLX5622-mediated depletion we observed is due to dosage of the drug and a combination

364 of direct effects on interstitial macrophages and indirect effects on replenishing monocytes.

365 Experiments that have examined sensitivity of lung macrophages to CSF1 uptake have

366 shown that interstitial macrophages more readily uptake CSF1 compared to alveolar

367 macrophages, despite similar expression of the CSF1R between the two populations [2].

368 This work suggests that although alveolar macrophages express CSF1R, they may be less

369 sensitive to CSF1R inhibitors and therefore resistant to depletion. In contrast, interstitial

370 macrophages may have a greater dependency on CSF1R signalling to regulate their

371 numbers and activation. Although the ontogeny of interstitial macrophages is somewhat

372 contested, these cells do appear to require some input from monocytes for their

373 maintenance and turnover. Monocyte turnover of interstitial macrophages has been shown

374 to occur at low levels although conflicting studies have indicated that both Ly6C^{hi} and

375 Ly6C^{low} subsets might play a role [27, 39]. In contrast, alveolar macrophages originate from

15

376 foetal monocytes and do not require peripheral turnover, maintaining their numbers via self-

377 renewal [37]. Whether PLX5622 interrupts monocyte replenishment of lung-resident

378 interstitial macrophages is unclear, although our data argue that monocytes were unable to

379 overcome PLX5622-mediated depletion even during infection, indicating that PLX5622 may

380 interrupt monocyte-mediated replenishment. The factors influencing replenishment and

381 contribution of monocytes to tissue-resident macrophage pools during infection is an

382 important avenue to explore in future studies.

383 Protection against *C. neoformans* infections largely depends on the action of

384 lymphocytes. IFNγ-producing CD4 T-cells are needed to prevent intracellular replication of

385 the fungus within monocytes and macrophages, and activate fungal killing pathways such as

386 induction of iNOS expression [17, 40]. B-cells produce antibodies which opsonise the fungus

387 and enable efficient phagocytosis, which is otherwise hampered by the presence of the

388 fungal capsule that shields against uptake by classic antifungal pattern recognition receptors

389 such as Dectin-1 [40]. Studies that explored the off-target effects of PLX5622 have reported

390 depletions of non-myeloid populations including T-cells and B-cells [11]. This has resulted in

391 controversy in the field as to whether these effects are widespread or due to concentration

392 and timing of PLX5622 treatment. We therefore extensively characterised lymphocyte

393 numbers in multiple tissues before and during fungal infection in PLX5622-treated mice.

394 However, we found no clear effects on the lymphoid population in PLX5622-treated mice, in

395 any of the tissues examined. We therefore attribute the reduction in fungal burdens observed

396 in PLX5622-treated mice to loss of myeloid cells and not any off-target effects on other cells

397 that do not express CSF1R.

398 Our work indicates that targeting CSF1R-dependent cells may protect against *C.*

399 *neoformans* infection. Susceptibility to *C. neoformans* infections in HIV-infected humans has

400 been partly attributed to the CSF1-CSF1R axis [41]. A recent genome-wide association

401 study found several polymorphisms upstream of the *CSF1* gene that associated with greater

402 susceptibility to cryptococcal meningitis in an African-based cohort of HIV-infected patients

403 [41]. Human PBMCs stimulated with heat-killed *C. neoformans* significantly upregulate *CSF1*

16

404   expression, and pre-treatment of PBMCs with CSF1 boosted uptake and killing of the fungus

405   [41]. Activation of monocytes/macrophages with CSF1 is therefore an important axis for

406   protection. However, our data indicate that macrophages dependent on CSF1 for survival

407   may instead promote infection, and targeting these cells with PLX5622 could be therapeutic.

408   Indeed, depletion of CSF1R-dependent disease-associated macrophages is a strategy

409   recently approved for treatment of tenosynovial giant cell tumours [42, 43]. PLX3397

410   (pexidartinib) removes CSF1R-dependent macrophages that contribute to the growth and

411   inflammation within these rare tumours [44]. Future studies should take into consideration

412   the potential beneficial and harmful effects of manipulating CSF1R signalling during *C.*

413   *neoformans* infection, which will likely be influenced organ- and timing-specific effects.

414   In summary, our data reveal that high dose PLX5622 treatment has a therapeutic

415   effect for *C. neoformans* infection by removing intracellular growth niches in the lung and

416   brain. We show that PLX5622 may be a useful strategy to deplete lung interstitial

417   macrophages, which we have used to demonstrate the importance of these cells in the

418   pathogenesis of *C. neoformans* lung infection and extrapulmonary dissemination.

17

419 **Methods**

420

421 **Mice**

422 8-12 week old C57BL/6 mice (males and females) were housed in individually ventilated cages

423 under specific pathogen free conditions at the Biomedical Services Unit at the University of

424 Birmingham, and had access to standard chow and drinking water *ad libitum*. Animal studies

425 were approved by the Animal Welfare and Ethical Review Board and UK Home Office under

426 Project Licence PBE275C33. Wild-type mice were purchased from Charles River. *Cx3cr1-*

427 *GFP-Ccr2-RFP* (strain number 032127) and *Nr4a1*$^{-/-}$ (strain number 006187) mice were

428 purchased from Jackson Laboratories and colonies bred and maintained at the University of

429 Birmingham. Mice were euthanised by cervical dislocation at indicated analysis time-points,

430 or when humane endpoints (e.g. 20% weight loss, hypothermia, meningitis) had been

431 reached, whichever occurred earlier.

432

433 **PLX5622 treatment**

434 PLX5622 (Plexxikon Inc. Berkley, CA) was formulated in AIN-76A rodent chow (Research

435 Diets) at a concentration of 1200 mg/kg. Mice were provided with PLX6522 diet or AIN-76A

436 control diet *ad libitum* for 1 week prior to infection, and continued throughout the infection

437 study period.

438

439 *C. neoformans* **growth and mouse infections**

440 *C. neoformans* strains used in this study were H99 and KN99α-mCherry [45]. Yeast was

441 routinely grown in YPD broth (2% peptone [Fisher Scientific], 2% glucose [Fisher Scientific],

442 and 1% yeast extract [Sigma]) at 30 °C for 24 hours at 200rpm. For infections, yeast cells were

443 washed twice in sterile PBS, counted using haemocytometer, and $2x10^5$ yeast (in 20μL)

444 pipetted onto the mouse nares under isoflurane anaesthesia. For analysis of organ fungal

445 burdens, animals were euthanized and organs weighed, homogenized in PBS, and serially

18

446   diluted before plating onto YPD agar supplemented with Penicillin/Streptomycin (Invitrogen).

447   Colonies were counted after incubation at 37°C for 48 hours.

448

449   ***C. neoformans* growth curve in PLX5622**

450   In some experiments, *C. neoformans* was grown in the presence of PLX5622 for 48 hours. *C.*

451   *neoformans* was seeded into 96 well plates at 5000 yeast/well, in the presence or absence of

452   PLX5622 (3-12µg/mL; see figure legends for final concentrations). Yeast growth was

453   monitored by serial readings at OD600 using a FLUOstar Omega microplate reader. Data was

454   averaged across 3 wells per growth condition.

455

456   **Isolation of brain leukocytes**

457   Leukocytes were isolated from brain using previously described methods [46]. Briefly, brains

458   were aseptically removed and stored in ice-cold FACS buffer (PBS + 0.5% BSA + 0.01%

459   sodium azide) prior to smashing into a paste using a syringe plunger. The suspension was

460   resuspended in 10mL 30% Percoll (GE Healthcare), and underlaid with 1.5mL of 70% Percoll.

461   Gradients were centrifuged at 2450 rpm for 30 min at 4 °C with the brake off. Leukocytes at

462   the interphase were collected and washed in FACS buffer prior to labelling with fluorophore-

463   conjugated antibodies and flow cytometry analysis.

464

465   **Meninges digestion**

466   The crown of the skull was aseptically removed and meninges were gently peeled from the

467   underside and collected in 1.5 Eppendorf containing 400µL digest buffer (RPMI

468   supplemented with 1mg/ml collagenase [Fisher scientific], 1mg/mL dispase [Sigma] and

469   40µg/mL DNAse [Sigma]). Meninges were digested in a 37 °C water bath for 30 minutes

470   with intermittent shaking every 5-10 minutes. The meninges were filtered through a 70µm

471   cell strainer and then centrifuged at 1500rpm for 5 min at 4°C. Cells were resuspended in

472   200µL FACS buffer and stored on ice prior to staining.

473

Isolation of lung leukocytes

Lungs were aseptically removed and placed in 4mL digest buffer (RPMI, 10% FBS, 1% Pen/Strep, 1mg/mL collagenase , 1mg/mL dispase and 40μg/mL DNase). The lungs were incubated in a water bath for 40-60 minutes at 37 °C with intermittent shaking every 5-10 min. Lung tissue then was gently smashed using a syringe plunger and filtered through 100µm filter. Lung cells were then collected by centrifugation at 1400rpm for 7 minutes at 4°C. Red blood cells were lysed on ice using PharmLyse solution (BD). Samples were washed in 2mM EDTA/PBS, filtered through at 40µm filter into a fresh tube, and collected by spinning at 1400rpm for 7 minutes. Cells were resuspended in 200µL FACS buffer, stored on ice, and placed in a FACS tube ready for staining.

Collection and preparation of peripheral blood

Mice were anesthetised with isoflurane and up to 300µL of peripheral blood obtained via cardiac puncture. Blood samples were missed 50µL of 100mM EDTA/PBS solution and kept on ice. Red blood cells were lysed on ice for 5 minutes using 5mL of PharmLyse solution (BD), with gentle inversion to mix after 2.5 minutes. 8mL of 2mM EDTA/PBS was added to each sample, gently inverted to mix, and cells collected by centrifugation at 1500rpm for 5 minutes at 4°C. The supernatant was discarded, and cells washed in FACS buffer prior to staining and analysis by flow cytometry.

Isolation of spleen leukocytes

Spleens were aseptically collected and placed in ice-cold PBS. For analysis of myeloid populations, spleens were digested in digest buffer (as above) for 30 minutes at 37ºC with intermittent shaking prior to smashing and washing. For analysis of lymphoid populations, spleens were directly smashed with a syringe plunger through a 70μm filter. Red blood cells were lysed on ice using PharmLyse solution (BD). Samples were washed in 2mM

500   EDTA/PBS, filtered through at 40μm filter into a fresh tube, and collected by spinning at

501   1500rpm for 5 minutes.

502

503   **Collection and preparation of bone marrow leukocytes**

504   Hind leg femurs were collected from mice and connective/muscle tissue removed. Ends of

505   the femur were removed using scissors, and bone marrow flushed out by passing 2mM

506   EDTA/PBS through the bone using a fine needle and syringe. Bone marrow was collected by

507   centrifugation, and red blood cells lysed using PharmLyse as above. Cells were washed in

508   FACS buffer prior to staining and analysis.

509

510   **Flow Cytometry**

511   Isolated leukocytes were resuspended in PBS and stained with Live/Dead stain (Invitrogen)

512   on ice as per manufacturer's instructions. Fc receptors were blocked with anti-CD16/32 and

513   staining with fluorophore-labelled antibodies was performed on ice for 15-60 minutes. Labelled

514   samples were acquired immediately or fixed in 2% paraformaldehyde prior to acquisition. In

515   some experiments, samples were fixed/permeabilised using the Foxp3 staining buffer set

516   (eBioscience) prior to intracellular staining for arginase (A1exF5, eBioscience) and Ki67

517   (16A8, Biolegend). Anti-mouse antibodies used in this study were: CD45 (30-F11), CD11b

518   (M1/70), CX3CR1 (SA011F11), MHC Class II (M5/114.15.2), F480 (BM8), Ly6G (1A8), Ly6C

519   (HK1.4), SiglecF (S1007L), CD64 (X54-5/7.1), CD206 (C068C2), all from Biolegend and

520   MerTK (D55MMER) from eBioscience. Samples were acquired on a BD LSR Fortessa

521   equipped with BD FACSDiva software. Analysis was performed using FlowJo (v10.6.1,

522   TreeStar).

523

524   **Measurement of cytokines in lung**

525   Lungs were stored in 1mL sterile PBS supplemented with 0.05% Tween20 and protease

526   inhibitor cocktail (Roche), then homogenised using a Stuart Handheld homogeniser (Cole

527   Parmer). Homogenates were centrifuged twice to remove debris and the supernatants snap-

21

528   frozen on dry ice and stored at -80ºC. Detection of IL-13 and IL-4 in lung homogenates was

529   determined using Duoset ELISA (R&D system) as per manufacturers instructions.

530

531   **Micro-computed tomography**

532   In these experiments, 9 week old BALB/cAn females were infected with 500 CFU of luciferase-

533   expressing *C. neoformans* KN99α [25]. Mice were anaesthetised with isoflurane (2.5% in

534   100% oxygen) and scanned in supine position using a dedicated small animal *in vivo* μCT

535   scanner (Skyscan 1278, Bruker micro-CT, Kontich, Belgium). The following parameters were

536   used: 50 kVp X-ray source voltage, 1 mm aluminium X-ray filter, 350 μA current, isotropic

537   reconstructed voxel size of 50 μm and 150 ms exposure time per projection with 0.9°

538   increments over a total of 220° angle, resulting in a total scanning time of ~3 min with

539   measured radiation dose of 60-80 mGy [47]. μCT-images were acquired weekly, from week 0

540   to week 4 post-infection. Software provided by the manufacturer (NRecon, DataViewer, and

541   CTan) was used to reconstruct, visualise, and process μCT data. For Hounsfield unit

542   calibration, a phantom of air-filled 1.5 mL tube located within a water-filled 50 mL tube was

543   scanned. For each animal at each timepoint, μCT-derived biomarkers of lung function and

544   pathology (aerated -, non-aerated -, and total lung volume) were quantified by manually

545   delineating a VOI on transverse images avoiding the heart and main blood vessels [48].

546

547   **Statistics**

548   Statistical analyses were performed using GraphPad Prism 9.0 software. Details of individual

549   tests are included in the figure legends. In general, data were tested for normal distribution

550   by Kolmogorov-Smirnov normality test and analyzed accordingly by unpaired two-tailed *t*-test

551   or Mann Whitney *U*-test. In cases where multiple data sets were analyzed, two-way ANOVA

552   was used with Bonferroni correction. In all cases, *P* values <0.05 were considered

553   significant.

References

1.   Dai X-M, Ryan GR, Hapel AJ, Dominguez MG, Russell RG, Kapp S, et al. Targeted disruption of the mouse colony-stimulating factor 1 receptor gene results in osteopetrosis, mononuclear phagocyte deficiency, increased primitive progenitor cell frequencies, and reproductive defects. Blood. 2002;99(1):111-20. doi: 10.1182/blood.V99.1.111.

2.   Hawley CA, Rojo R, Raper A, Sauter KA, Lisowski ZM, Grabert K, et al. Csf1r-mApple Transgene Expression and Ligand Binding In Vivo Reveal Dynamics of CSF1R Expression within the Mononuclear Phagocyte System. Journal of immunology (Baltimore, Md : 1950). 2018;200(6):2209-23. Epub 2018/02/12. doi: 10.4049/jimmunol.1701488. PubMed PMID: 29440354.

3.   Pridans C, Raper A, Davis GM, Alves J, Sauter KA, Lefevre L, et al. Pleiotropic Impacts of Macrophage and Microglial Deficiency on Development in Rats with Targeted Mutation of the Csf1r Locus. The Journal of Immunology. 2018;201(9):2683. doi: 10.4049/jimmunol.1701783.

4.   Oosterhof N, Chang IJ, Karimiani EG, Kuil LE, Jensen DM, Daza R, et al. Homozygous Mutations in CSF1R Cause a Pediatric-Onset Leukoencephalopathy and Can Result in Congenital Absence of Microglia. Am J Hum Genet. 2019;104(5):936-47. Epub 2019/04/16. doi: 10.1016/j.ajhg.2019.03.010. PubMed PMID: 30982608; PubMed Central PMCID: PMCPMC6506793.

5.   Rojo R, Raper A, Ozdemir DD, Lefevre L, Grabert K, Wollscheid-Lengeling E, et al. Deletion of a Csf1r enhancer selectively impacts CSF1R expression and development of tissue macrophage populations. Nature Communications. 2019;10(1):3215. doi: 10.1038/s41467-019-11053-8.

6.   Han J, Harris RA, Zhang XM. An updated assessment of microglia depletion: current concepts and future directions. Mol Brain. 2017;10(1):25. Epub 2017/06/21. doi: 10.1186/s13041-017-0307-x. PubMed PMID: 28629387; PubMed Central PMCID: PMCPMC5477141.

589   7.   Liu Y, Given KS, Dickson EL, Owens GP, Macklin WB, Bennett JL. Concentration-

590   dependent effects of CSF1R inhibitors on oligodendrocyte progenitor cells ex vivo and in

591   vivo. Exp Neurol. 2019;318:32-41. Epub 2019/04/29. doi: 10.1016/j.expneurol.2019.04.011.

592   PubMed PMID: 31029597; PubMed Central PMCID: PMCPMC6615458.

593   8.   Spangenberg E, Severson PL, Hohsfield LA, Crapser J, Zhang J, Burton EA, et al.

594   Sustained microglial depletion with CSF1R inhibitor impairs parenchymal plaque

595   development in an Alzheimer's disease model. Nature Communications. 2019;10(1):3758.

596   doi: 10.1038/s41467-019-11674-z.

597   9.   Wheeler DL, Sariol A, Meyerholz DK, Perlman S. Microglia are required for protection

598   against lethal coronavirus encephalitis in mice. J Clin Invest. 2018;128(3):931-43. doi:

599   10.1172/JCI97229.

600   10.   Feng X, Valdearcos M, Uchida Y, Lutrin D, Maze M, Koliwad SK. Microglia mediate

601   postoperative hippocampal inflammation and cognitive decline in mice. JCI Insight.

602   2017;2(7):e91229. Epub 2017/04/14. doi: 10.1172/jci.insight.91229. PubMed PMID:

603   28405620; PubMed Central PMCID: PMCPMC5374063 exists.

604   11.   Lei F, Cui N, Zhou C, Chodosh J, Vavvas Demetrios G, Paschalis Eleftherios I.

605   CSF1R inhibition by a small-molecule inhibitor is not microglia specific; affecting

606   hematopoiesis and the function of macrophages. Proceedings of the National Academy of

607   Sciences. 2020;117(38):23336-8. doi: 10.1073/pnas.1922788117.

608   12.   Green KN, Hume DA. On the utility of CSF1R inhibitors. Proceedings of the National

609   Academy of Sciences. 2021;118(4):e2019695118. doi: doi:10.1073/pnas.2019695118.

610   13.   Feng X, Jopson TD, Paladini MS, Liu S, West BL, Gupta N, et al. Colony-stimulating

611   factor 1 receptor blockade prevents fractionated whole-brain irradiation-induced memory

612   deficits. Journal of Neuroinflammation. 2016;13(1):215. doi: 10.1186/s12974-016-0671-y.

613   14.   Schwarzer P, Kokona D, Ebneter A, Zinkernagel MS. Effect of Inhibition of Colony-

614   Stimulating Factor 1 Receptor on Choroidal Neovascularization in Mice. The American

615   Journal of Pathology. 2020;190(2):412-25. doi: https://doi.org/10.1016/j.ajpath.2019.10.011.

616   15.   Nissen JC, Thompson KK, West BL, Tsirka SE. Csf1R inhibition attenuates

617   experimental autoimmune encephalomyelitis and promotes recovery. Exp Neurol.

618   2018;307:24-36. Epub 2018/05/29. doi: 10.1016/j.expneurol.2018.05.021. PubMed PMID:

619   29803827; PubMed Central PMCID: PMCPMC6380683.

620   16.   Paschalis EI, Lei F, Zhou C, Kapoulea V, Dana R, Chodosh J, et al. Permanent

621   neuroglial remodeling of the retina following infiltration of CSF1R inhibition-resistant

622   peripheral monocytes. Proceedings of the National Academy of Sciences.

623   2018;115(48):E11359-E68. doi: doi:10.1073/pnas.1807123115.

624   17.   Mohamed SH, Nyazika TK, Ssebambulidde K, Lionakis MS, Meya DB, Drummond

625   RA. Fungal CNS Infections in Africa: The Neuroimmunology of Cryptococcal Meningitis.

626   Front Immunol. 2022;13. doi: 10.3389/fimmu.2022.804674.

627   18.   Rajasingham R, Govender NP, Jordan A, Loyse A, Shroufi A, Denning DW, et al.

628   The global burden of HIV-associated cryptococcal infection in adults in 2020: a modelling

629   analysis. Lancet Infect Dis. 2022. doi: https://doi.org/10.1016/S1473-3099(22)00499-6.

630   19.   Sun D, Zhang M, Sun P, Liu G, Strickland AB, Chen Y, et al. VCAM1/VLA4

631   interaction mediates Ly6Clow monocyte recruitment to the brain in a TNFR signaling

632   dependent manner during fungal infection. PLOS Pathogens. 2020;16(2):e1008361. doi:

633   10.1371/journal.ppat.1008361.

634   20.   Santiago-Tirado FH, Onken MD, Cooper JA, Klein RS, Doering TL. Trojan Horse

635   Transit Contributes to Blood-Brain Barrier Crossing of a Eukaryotic Pathogen. mBio.

636   2017;8(1). doi: 10.1128/mBio.02183-16.

637   21.   Mohamed SH, Fu MS, Hain S, Alselami A, Vanhoffelen E, Li Y, et al. Microglia

638   protect fungi against copper starvation and promote brain infection. bioRxiv.

639   2022:2022.09.07.506901. doi: 10.1101/2022.09.07.506901.

640   22.   Dang EV, Lei S, Radkov A, Volk RF, Zaro BW, Madhani HD. Secreted fungal

641   virulence effector triggers allergic inflammation via TLR4. Nature. 2022;608(7921):161-7.

642   Epub 2022/07/28. doi: 10.1038/s41586-022-05005-4. PubMed PMID: 35896747.

643   23.   Wolf AA, Yáñez A, Barman PK, Goodridge HS. The Ontogeny of Monocyte Subsets.

644   Frontiers in Immunology. 2019;10. doi: 10.3389/fimmu.2019.01642.

645   24.   Elmore MRP, Hohsfield LA, Kramár EA, Soreq L, Lee RJ, Pham ST, et al.

646   Replacement of microglia in the aged brain reverses cognitive, synaptic, and neuronal

647   deficits in mice. Aging Cell. 2018;17(6):e12832. Epub 2018/10/03. doi: 10.1111/acel.12832.

648   PubMed PMID: 30276955; PubMed Central PMCID: PMCPMC6260908.

649   25.   Vanherp L, Ristani A, Poelmans J, Hillen A, Lagrou K, Janbon G, et al. Sensitive

650   bioluminescence imaging of fungal dissemination to the brain in mouse models of

651   cryptococcosis. Disease models & mechanisms [Internet]. 2019 2019/06//;

652   12(6):[dmm039123 p.]. Available from: http://europepmc.org/abstract/MED/31101657

653   https://doi.org/10.1242/dmm.039123

654   https://europepmc.org/articles/PMC6602310.

655   26.   Ural BB, Yeung ST, Damani-Yokota P, Devlin JC, de Vries M, Vera-Licona P, et al.

656   Identification of a nerve-associated, lung-resident interstitial macrophage subset with distinct

657   localization and immunoregulatory properties. Sci Immunol. 2020;5(45). Epub 2020/03/30.

658   doi: 10.1126/sciimmunol.aax8756. PubMed PMID: 32220976; PubMed Central PMCID:

659   PMCPMC7717505.

660   27.   Schyns J, Bai Q, Ruscitti C, Radermecker C, De Schepper S, Chakarov S, et al.

661   Non-classical tissue monocytes and two functionally distinct populations of interstitial

662   macrophages populate the mouse lung. Nature Communications. 2019;10(1):3964. doi:

663   10.1038/s41467-019-11843-0.

664   28.   Jenkins SJ, Ruckerl D, Thomas GD, Hewitson JP, Duncan S, Brombacher F, et al.

665   IL-4 directly signals tissue-resident macrophages to proliferate beyond homeostatic levels

666   controlled by CSF-1. J Exp Med. 2013;210(11):2477-91. Epub 2013/10/09. doi:

667   10.1084/jem.20121999. PubMed PMID: 24101381; PubMed Central PMCID:

668   PMCPMC3804948.

669   29.   Ben-Abdallah M, Sturny-Leclère A, Avé P, Louise A, Moyrand F, Weih F, et al.

670   Fungal-induced cell cycle impairment, chromosome instability and apoptosis via differential

671   activation of NF-κB. PLoS Pathog. 2012;8(3):e1002555. Epub 2012/03/08. doi:

672   10.1371/journal.ppat.1002555. PubMed PMID: 22396644; PubMed Central PMCID:

673   PMCPMC3291658.

674   30.   Hanna RN, Carlin LM, Hubbeling HG, Nackiewicz D, Green AM, Punt JA, et al. The

675   transcription factor NR4A1 (Nur77) controls bone marrow differentiation and the survival of

676   Ly6C- monocytes. Nat Immunol. 2011;12(8):778-85. Epub 2011/07/05. doi: 10.1038/ni.2063.

677   PubMed PMID: 21725321; PubMed Central PMCID: PMCPMC3324395.

678   31.   Prinz M, Erny D, Hagemeyer N. Ontogeny and homeostasis of CNS myeloid cells.

679   Nat Immunol. 2017;18(4):385-92. doi: 10.1038/ni.3703.

680   32.   Zhou X, Ballou ER. The Cryptococcus neoformans Titan Cell: From In Vivo

681   Phenomenon to In Vitro Model. Current Clinical Microbiology Reports. 2018;5(4):252-60. doi:

682   10.1007/s40588-018-0107-9.

683   33.   Dambuza IM, Drake T, Chapuis A, Zhou X, Correia J, Taylor-Smith L, et al. The

684   Cryptococcus neoformans Titan cell is an inducible and regulated morphotype underlying

685   pathogenesis. PLOS Pathogens. 2018;14(5):e1006978. doi: 10.1371/journal.ppat.1006978.

686   34.   Denham ST, Brammer B, Chung KY, Wambaugh MA, Bednarek JM, Guo L, et al. A

687   dissemination-prone morphotype enhances extrapulmonary organ entry by Cryptococcus

688   neoformans. Cell Host Microbe. 2022. Epub 2022/09/14. doi: 10.1016/j.chom.2022.08.017.

689   PubMed PMID: 36099922.

690   35.   Charlier C, Nielsen K, Daou S, Brigitte M, Chretien F, Dromer F. Evidence of a role

691   for monocytes in dissemination and brain invasion by Cryptococcus neoformans. Infect

692   Immun. 2009;77(1):120-7. Epub 2008/10/22. doi: 10.1128/iai.01065-08. PubMed PMID:

693   18936186; PubMed Central PMCID: PMCPMC2612285.

694   36.   Heung LJ, Hohl TM. Inflammatory monocytes are detrimental to the host immune

695   response during acute infection with Cryptococcus neoformans. PLOS Pathogens.

696   2019;15(3):e1007627. doi: 10.1371/journal.ppat.1007627.

697   37.   Bain CC, MacDonald AS. The impact of the lung environment on macrophage

698   development, activation and function: diversity in the face of adversity. Mucosal Immunology.

699   2022;15(2):223-34. doi: 10.1038/s41385-021-00480-w.

700   38.   Aegerter H, Kulikauskaite J, Crotta S, Patel H, Kelly G, Hessel EM, et al. Influenza-

701   induced monocyte-derived alveolar macrophages confer prolonged antibacterial protection.

702   Nat Immunol. 2020;21(2):145-57. Epub 2020/01/15. doi: 10.1038/s41590-019-0568-x.

703   PubMed PMID: 31932810; PubMed Central PMCID: PMCPMC6983324.

704   39.   Chakarov S, Lim HY, Tan L, Lim SY, See P, Lum J, et al. Two distinct interstitial

705   macrophage populations coexist across tissues in specific subtissular niches. Science.

706   2019;363(6432):eaau0964. doi: 10.1126/science.aau0964.

707   40.   Campuzano A, Wormley FL. Innate Immunity against Cryptococcus, from

708   Recognition to Elimination. Journal of Fungi. 2018;4(1):33. PubMed PMID:

709   doi:10.3390/jof4010033.

710   41.   Kannambath S, Jarvis JN, Wake RM, Longley N, Loyse A, Matzaraki V, et al.

711   Genome-Wide Association Study Identifies Novel Colony Stimulating Factor 1 Locus

712   Conferring Susceptibility to Cryptococcosis in Human Immunodeficiency Virus-Infected

713   South Africans. Open Forum Infect Dis. 2020;7(11):ofaa489. Epub 2020/12/04. doi:

714   10.1093/ofid/ofaa489. PubMed PMID: 33269293; PubMed Central PMCID:

715   PMCPMC7686661.

716   42.   Gelderblom H, Wagner AJ, Tap WD, Palmerini E, Wainberg ZA, Desai J, et al. Long-

717   term outcomes of pexidartinib in tenosynovial giant cell tumors. Cancer. 2021;127(6):884-93.

718   Epub 2020/11/17. doi: 10.1002/cncr.33312. PubMed PMID: 33197285; PubMed Central

719   PMCID: PMCPMC7946703.

720   43.   Gelderblom H, de Sande Mv. Pexidartinib: first approved systemic therapy for

721   patients with tenosynovial giant cell tumor. Future Oncology. 2020;16(29):2345-56. doi:

722   10.2217/fon-2020-0542.

723   44.   Benner B, Good L, Quiroga D, Schultz TE, Kassem M, Carson WE, et al.

724   Pexidartinib, a Novel Small Molecule CSF-1R Inhibitor in Use for Tenosynovial Giant Cell

725 Tumor: A Systematic Review of Pre-Clinical and Clinical Development. Drug Des Devel

726 Ther. 2020;14:1693-704. Epub 2020/05/23. doi: 10.2147/dddt.S253232. PubMed PMID:

727 32440095; PubMed Central PMCID: PMCPMC7210448.

728 45.   Voelz K, Johnston SA, Rutherford JC, May RC. Automated analysis of cryptococcal

729 macrophage parasitism using GFP-tagged cryptococci. PLoS One. 2010;5(12):e15968.

730 Epub 2011/01/07. doi: 10.1371/journal.pone.0015968. PubMed PMID: 21209844; PubMed

731 Central PMCID: PMCPMC3013146 PLoS ONE.

732 46.   Lionakis MS, Lim JK, Lee CCR, Murphy PM. Organ-specific innate immune

733 responses in a mouse model of invasive candidiasis. J Innate Immun. 2011;3(2):180-99. doi:

734 10.1159/000321157. PubMed PMID: WOS:000287559700008.

735 47.   Berghen N, Dekoster K, Marien E, Dabin J, Hillen A, Wouters J, et al. Radiosafe

736 micro-computed tomography for longitudinal evaluation of murine disease models. Scientific

737 Reports. 2019;9(1):17598. doi: 10.1038/s41598-019-53876-x.

738 48.   Vande Velde G, Poelmans J, De Langhe E, Hillen A, Vanoirbeek J, Himmelreich U,

739 et al. Longitudinal micro-CT provides biomarkers of lung disease that can be used to assess

740 the effect of therapy in preclinical mouse models, and reveal compensatory changes in lung

741 volume. Disease Models & Mechanisms. 2016;9(1):91-8. doi: 10.1242/dmm.020321.

742

Figures and Legends
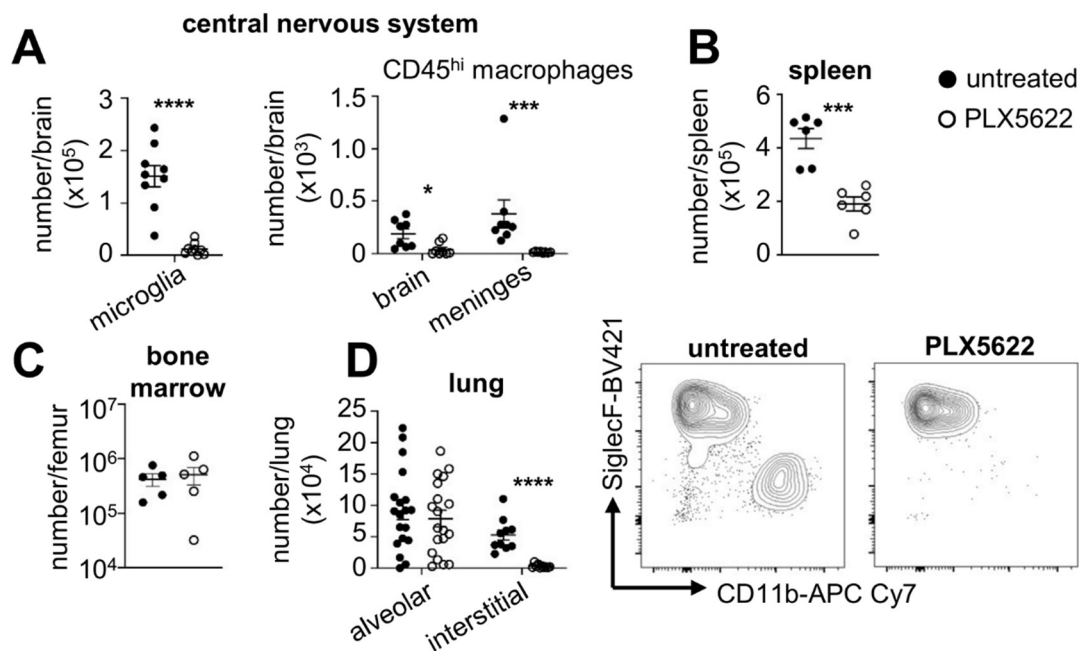
Figure 1: PLX5622 depletes macrophages within the CNS, spleen and lung. Wild-type C57BL/6 mice were given PLX5622 diet (1200ppm) or control diet for 7 days prior to measurement of macrophage numbers in (A) brain and meninges (microglia n=9 per group; macrophages n=8 per group), (B) spleen (n=6 mice per group) and (C) lung (alveolar n=19 per group; interstitial n=10 per group) by flow cytometry. Example lung plots are gated on live CD45+CD64+MerTK+ singlets. Gating strategies for each macrophage population is shown in Fig S1. Data is pooled from 2-4 independent experiments and analysed by unpaired t-tests. ***P<0.005, ****P<0.0001.

754
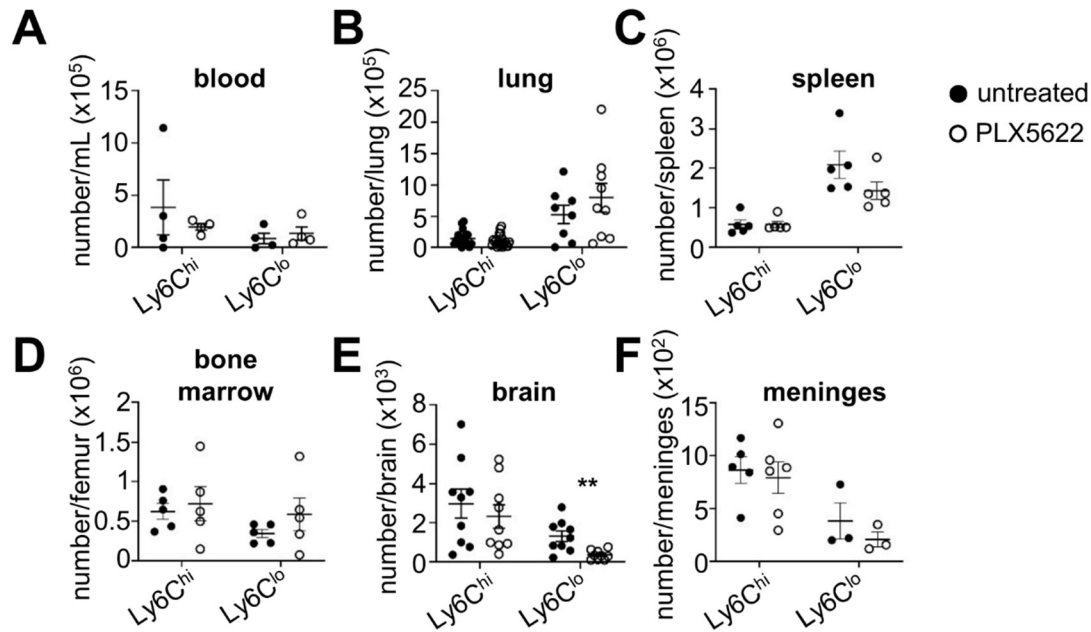
Figure 2: CNS-infiltrating Ly6C^{low} monocytes are depleted in PLX5622-treated mice.

Wild-type C57BL/6 mice were given PLX5622 diet (1200ppm) or control diet for 7 days prior

to measurement of monocyte numbers in (A) blood (n=4 per group), (B) lung (Ly6C^{hi}

monocytes n=19 per group; Ly6C^{low} monocytes n=9 per group), (C) brain (n=9 per group) by

flow cytometry. Gating strategies for each monocyte population is shown in Fig S1. Data is

pooled from 2-4 independent experiments and analysed by unpaired t-tests.

761
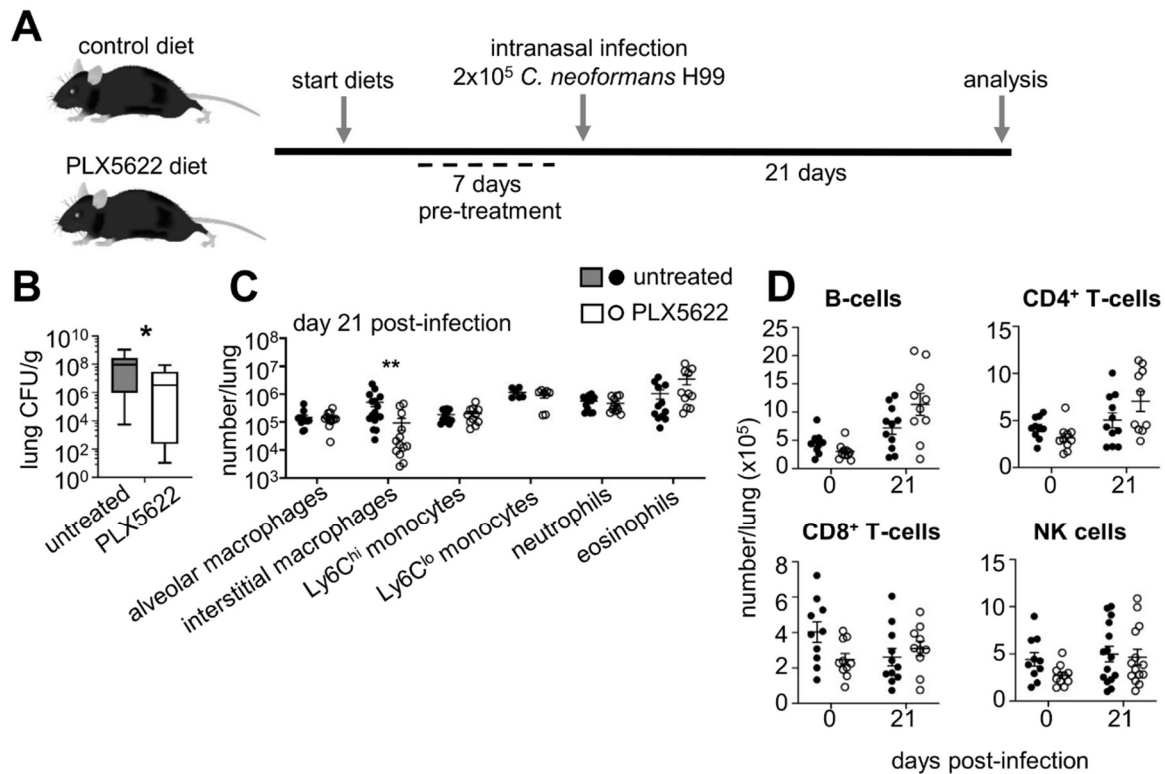
Figure 3: PLX5622 treatment reduces *C. neoformans* lung infection. (A) Schematic of PLX5622 treatment and infection model. Wild-type C57BL/6 mice were pre-treated for 7 days with PLX5622 diet or control diet, then infected intranasally with *C. neoformans*. Mice were analysed up to 21 days post-infection, control and PLX5622 diets were maintained throughout. (B) Lung fungal burdens at day 21 post-infection in untreated (n=10) and PLX5622-treated (n=10) mice. Data pooled from 2 independent experiments and analysed by Mann Whitney U-test, *P<0.05. (C) Flow cytometry was used to determine number of indicated immune cells in the lung at day 21 post-infection (n=12-16 per group). Data is pooled from 3-4 independent experiments and analysed by two-way ANOVA, **P<0.01. (D) Flow cytometry was used to determine the number of indicated lymphocyte populations in the lungs of uninfected (n=10 per group) and at day 21 post-infection (n=10-11 per group) of untreated and PLX5622-treated mice. Data is pooled from 2-3 independent experiments.

33

774
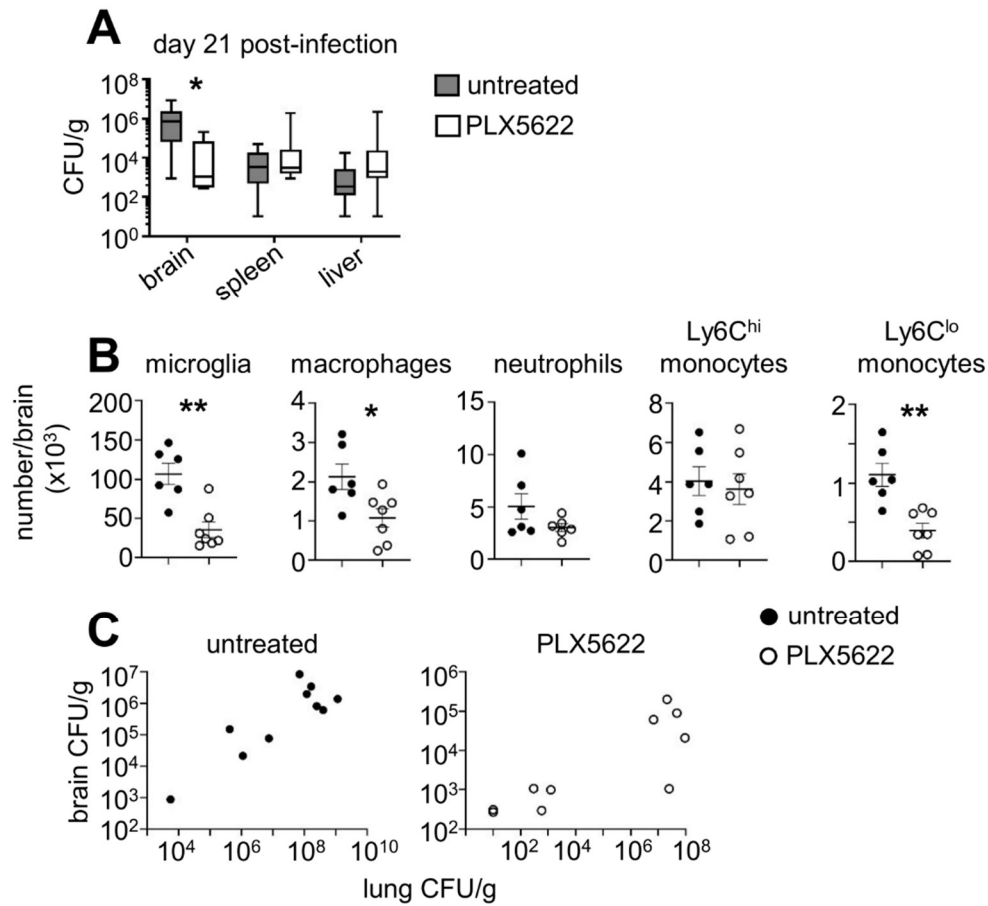
Figure 4: PLX5622 treatment reduces fungal brain infection. (A) Fungal burdens in the indicated organs at day 21 post-infection in untreated and PLX5622-treated mice (brain n=10 mice per group; liver/spleen n=7 mice per group). Data pooled from 2-3 independent experiments and analysed by Mann Whitney U-tests. *P<0.05. (B) Total numbers of indicated myeloid cells in the brain of untreated (n=6) and PLX5622-treated (n=7) mice at day 21 post-infection. Data is pooled from 2 independent experiments and analysed by unpaired t-tests. *P<0.05, **P<0.01. (C) Correlation between fungal burdens in lung and brain of same mice that were either untreated (n=10) or PLX5622-treated (n=10) at day 21 post-infection. Data pooled from 2 independent experiments.
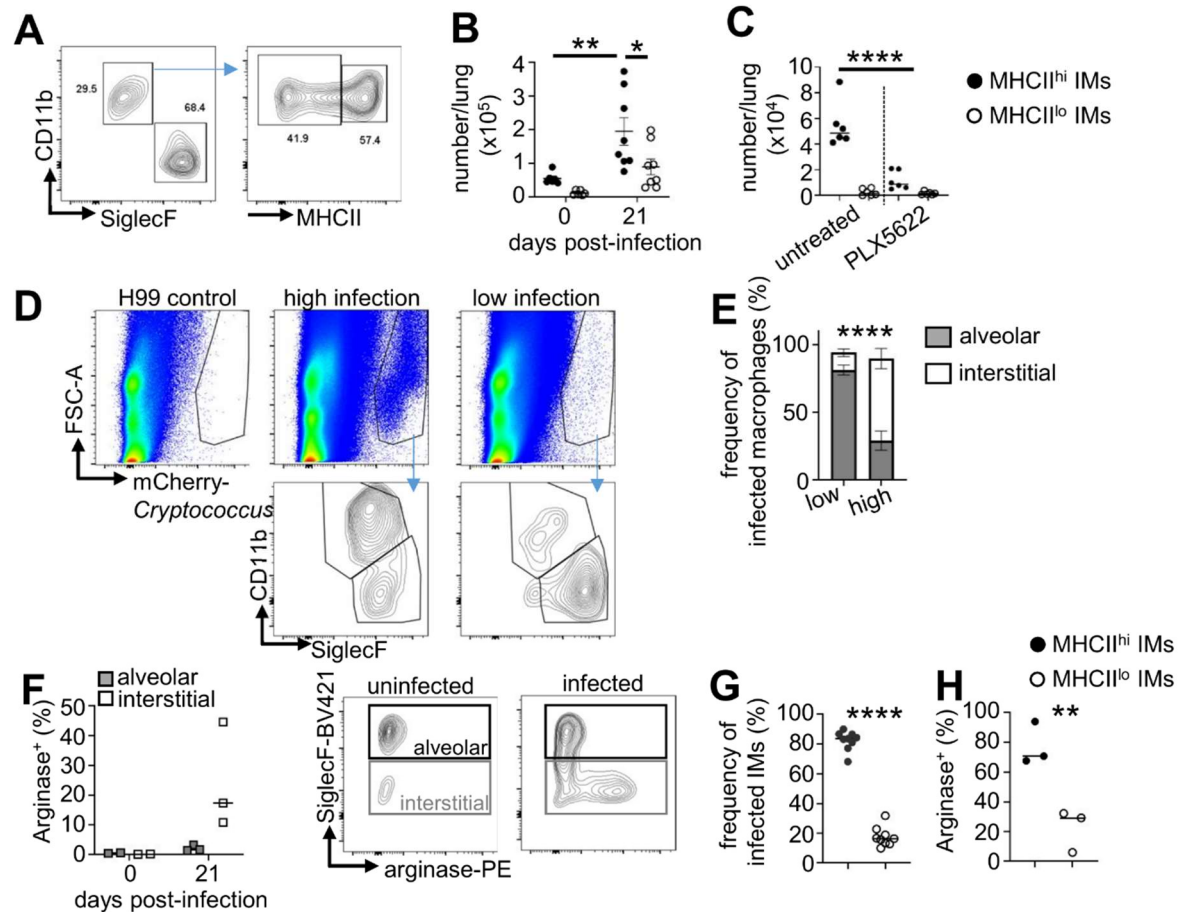
Figure 5: MHCII^{hi} interstitial lung macrophages are susceptible to *C. neoformans*

infection. (A) Example flow cytometry of interstitial macrophage gating strategy used in this

study. (B) Total number of MHCII^{hi} and MHCII^{low} interstitial macrophages in the lung of

uninfected (n=6 per group) and infected (n=8 per group) mice. Data pooled from 2

independent experiments and analysed by two-way ANOVA. *P<0.05, **P<0.01. (C) Total

number of interstitial macrophage subsets in the lung of uninfected mice that were either

untreated (n=6 mice) or PLX5622-treated (n=6 mice). Data pooled from 2 independent

experiments and analysed by one-way ANOVA. ****P<0.0001. (D) Example plots showing

ungated lung samples from mice infected with non-fluorescent *C. neoformans* (H99; gating

control), and mice infected with mCherry-*C. neoformans* that were grouped as having 'high

infection' or 'low infection'. Yeast were further gated as CD45$^+$CD64$^+$MerTK$^+$ to isolate

infected macrophages, which were further split into alveolar and interstitial macrophage

populations (bottom row). (E) Frequency of infected alveolar and interstitial macrophages

798 (within total infected macrophage gate, CD45$^+$CD64$^+$MerTK$^+$) in mice (n=9 total) with high

799 (n=3) or low (n=6) infection of the lung. Data pooled from 3 independent experiments and

800 analysed by two-way ANOVA. ****P<0.0001. (F) Frequency of arginase expression within

801 alveolar and interstitial macrophages in uninfected (n=2 mice per group) and infected (n=3

802 mice per group). Example plots are gated on CD64$^+$MerTK$^+$ macrophages. Data is from a

803 single experiment. (G) Frequency of *C. neoformans* infection within MHCII^{hi} and MHCII^{low}

804 interstitial macrophages (within total infected interstitial macrophages). Data pooled from 3

805 independent experiments (n=9 total mice), and analysed by unpaired t-test. ****P<0.0001.

806 (H) Frequency of arginase expression in MHCII^{hi} and MHCII^{low} interstitial macrophages in the

807 *C. neoformans* infected lung. Data is from a single experiment (n=3 mice per group).
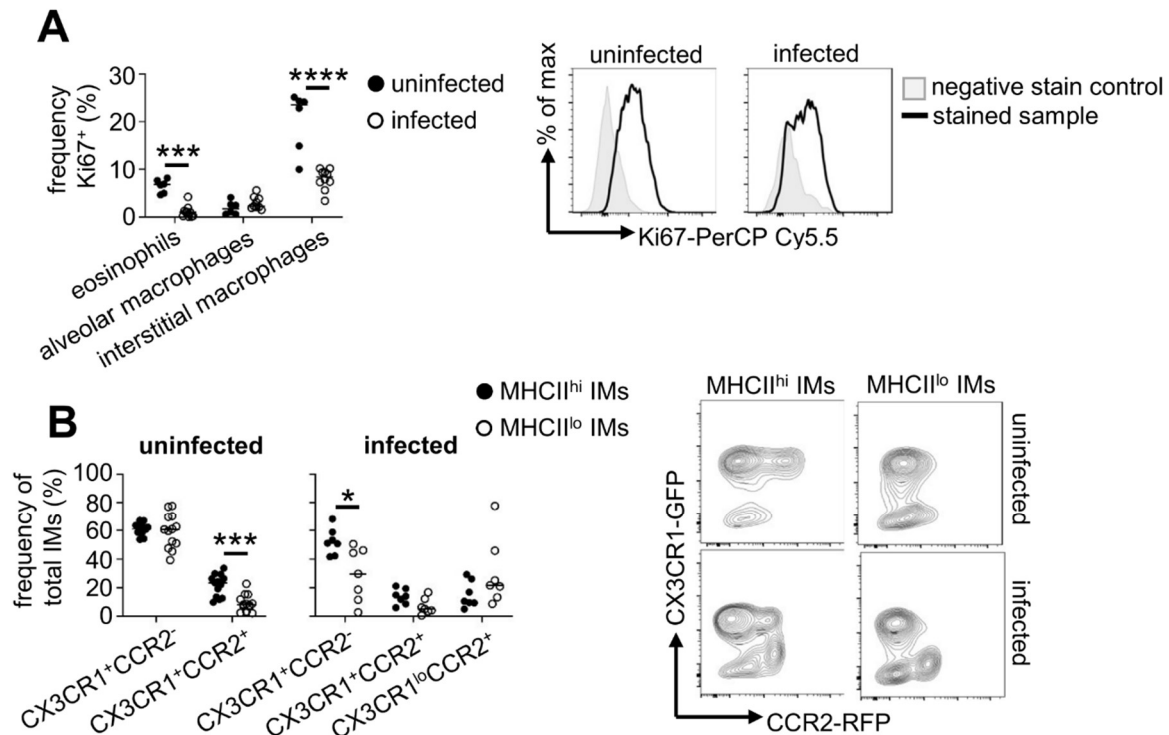
Figure 6: Interstitial macrophage expansion during *C. neoformans* infection is due to monocyte replenishment and not local division. (A) Frequency of proliferating (Ki67+) eosinophils, alveolar and interstitial macrophages in the lungs of uninfected (n=6) and at day 21 post-infection (n=9) mice. Example histograms are gated on interstitial macrophages for infected lung stained with Ki67 (black line) or the fluorescence minus one control (grey filled histogram). Data is pooled from 2 independent experiments and analysed by two-way ANOVA. ***P<0.005, ****P<0.0001. (B) Frequency of interstitial macrophages positive for CX3CR1 and CCR2 expression in the uninfected (n=13 mice) and day 21 post-infected lung (n=7 mice). Example plots are gated on the indicated interstitial macrophage sub-populations. Data is pooled from 2-3 independent experiments and analysed by two-way ANOVA. *P<0.05, ***P<0.005.

821
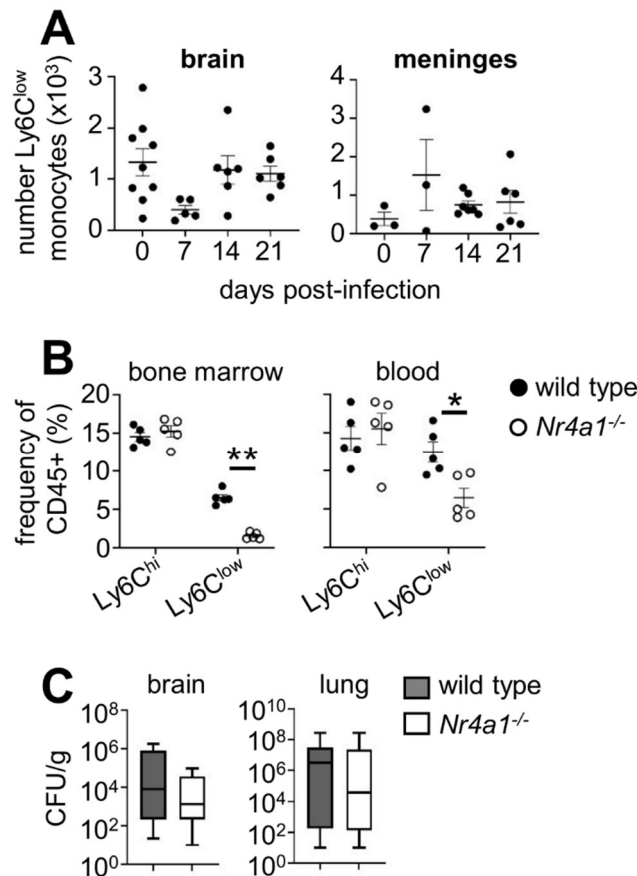
Figure 7: Patrolling monocytes play a redundant role in control and dissemination of pulmonary *C. neoformans* infections. (A) Total number of Ly6C^{low} patrolling monocytes in the brain and meninges of wild-type C57BL/6 mice at indicated time points post-intranasal infection. Each point represents a single animal. Data is pooled from 1 (meninges) or 2 (brain) independent experiments. (B) Frequency of Ly6C^{hi} and Ly6C^{low} monocytes in the bone marrow and peripheral blood of uninfected *Nr4a1*$^{-/-}$ (n=5 mice) and wild-type controls (n=5 mice). Data from a single experiment and analysed by two-way ANOVA. *$P<0.05$, **$P<0.01$. (C) Fungal burdens in the brain and lung at day 21 post-infection in wild-type (n=19) and *Nr4a1*$^{-/-}$ (n=20) mice. Data pooled from 3 independent experiments.

831

832   **Supplementary Figures**

833
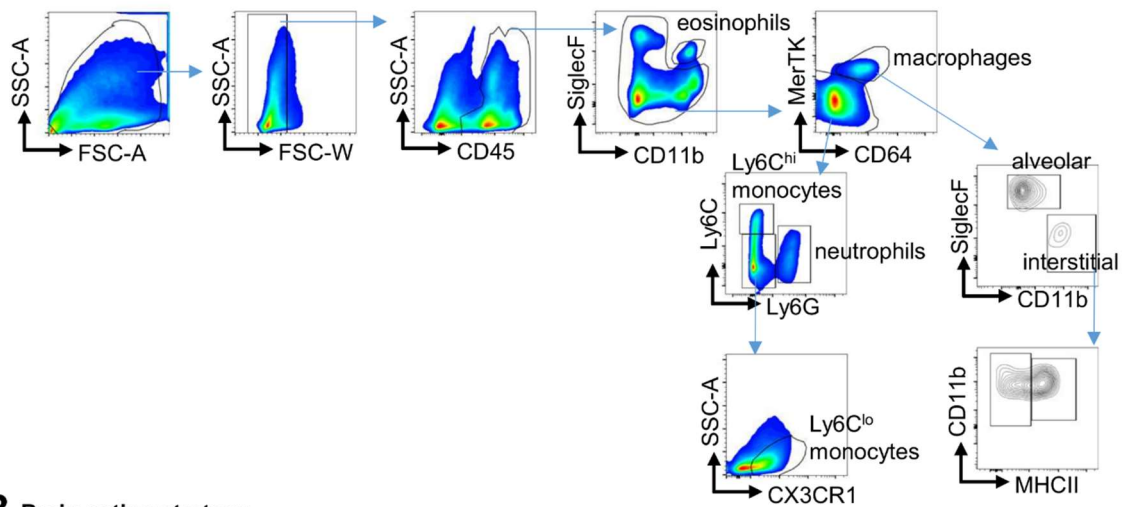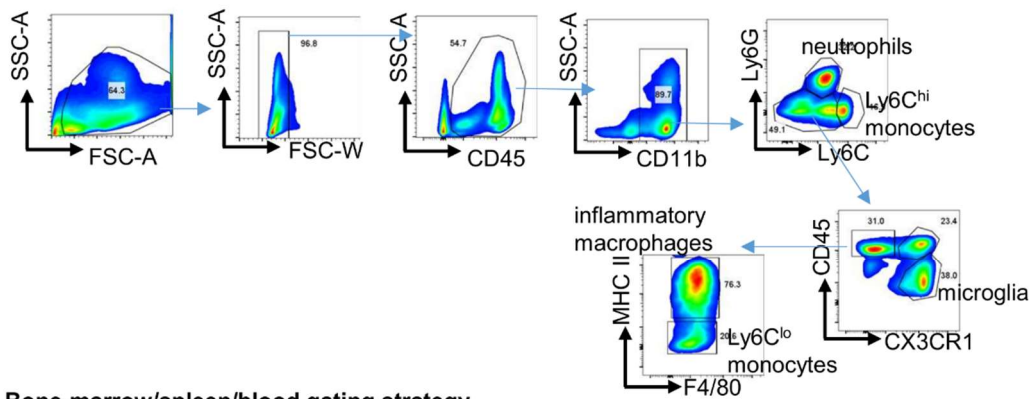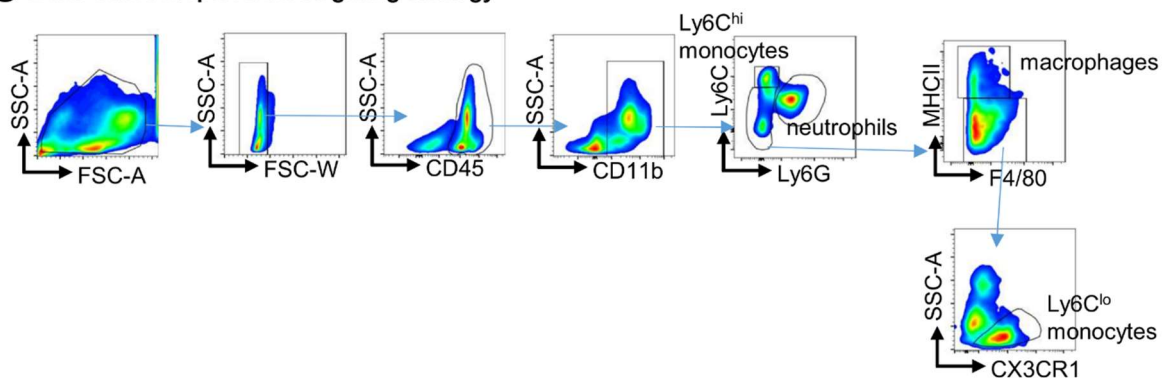
834   **Figure S1: Gating strategies used in this study.** Basic gating strategy used to define

835   myeloid cell populations in the (A) lung, (B) brain and (C) spleen, bone marrow and blood.
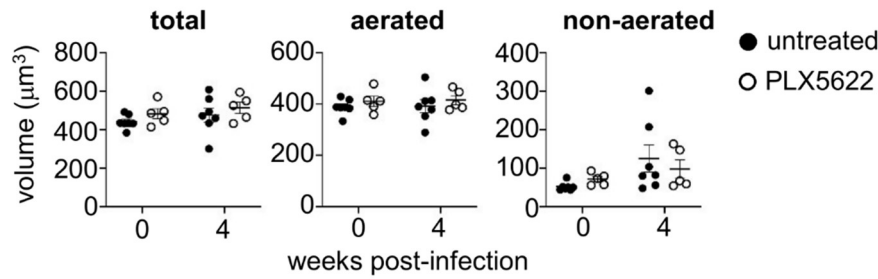
836

837

838

Figure S2: PLX5622 does not affect lung volume or aeration. Total lung volume, aerated

lung volume and non-aerated lung (corresponding to lesion) volume were quantified from

μCT images in mice that were untreated (n= 7 mice) or PLX5622 treated (n = 5 mice) at

baseline (7 days post-diet, no infection) and 4 weeks post-infection. Data is pooled from 2

independent experiments.

844
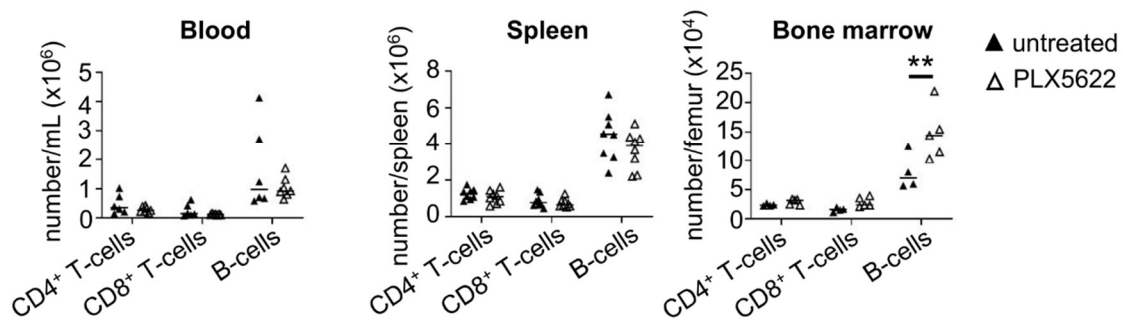
Figure S3: PLX5622 does not affect numbers of circulating lymphocytes. Total number

of CD4+ T-cells, CD8+ T-cells and B-cells in the indicated organs of untreated (n=4-6 mice)

and PLX5622-treated (n=5-8 mice) wild-type mice (all uninfected). Data is from 1 (bone

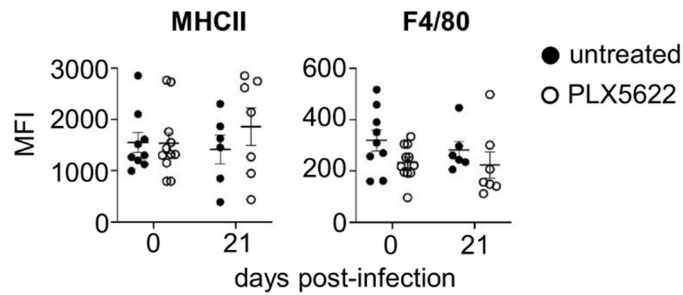marrow) or pooled from 2 independent experiments (blood, spleen).

849

850

851

Figure S4: PLX5622 does not affect expression of MHCII or F4/80 by alveolar macrophages. Mean fluorescent intensity of MHCII and F4/80 by alveolar macrophages in the untreated (n = 6-9 mice) and PLX5622-treated (n = 7-10 mice) lung at the indicated time points relative to C. neoformans infection. Data pooled from 2-3 independent experiments.

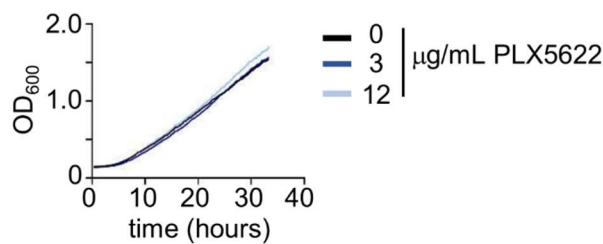856

857

Figure S5: PLX5622 does not affect fungal growth directly. Growth curve of *C. neoformans* grown in the indicated concentrations of PLX5622. Data is representative of 2 independent experiments.
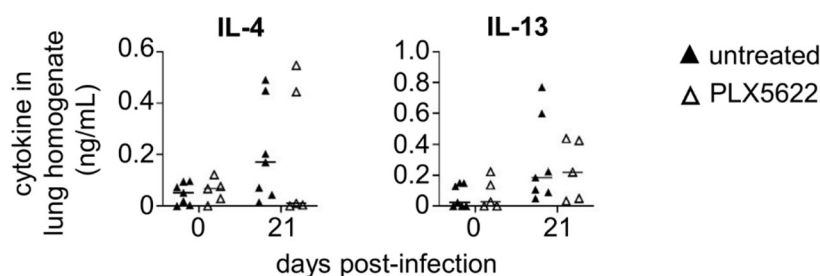
861

862

863

Figure S6: PLX5622 does not affect production of IL-4 and IL-13 within the lung. Concentration of IL-4 and IL-13 was measured in total lung homogenates of uninfected and

41

866   infected mice, either untreated (n= 7 mice) or PLX5622-treated (n= 5 mice). Data pooled

867   from 2 independent experiments.
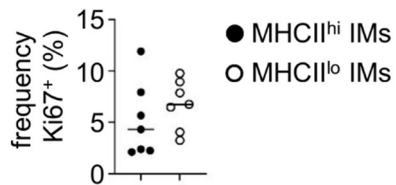
868

869

870   **Figure S7: Interstitial macrophage subsets do not differ in Ki67 labelling.** Frequency of

871   Ki67+ interstitial lung macrophages that were either MHCII^{hi} or MHCII^{lo}. IM = interstitial

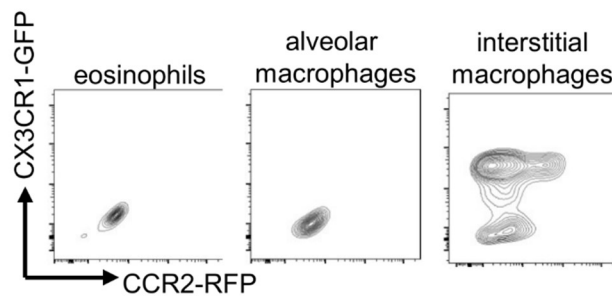872   macrophage. Data pooled from 2 independent experiments (n= 7 mice).

873

874

875   **Figure S8:** Background expression levels of CX3CR1 and CCR2 in the indicated cell types

876   within the infected lung.